Nanocomposites from Fluoro-Oxygenated Polyethylene: A Novel Route to Organoclay Exfoliation

Rhutesh K. Shah,[1] Lili Cui,[1] Kelly L. Williams,[2] Bernard Bauman,[2] D. R. Paul[1]

[1]*Department of Chemical Engineering and Texas Materials Institute, University of Texas at Austin, Austin, Texas 78712*
[2]*Inhance Fluoro-Seal, 16360 Park Ten Place, Suite 325, Houston, Texas 77084*

Received 6 November 2005; accepted 4 April 2006
DOI 10.1002/app.24586
Published online in Wiley InterScience (www.interscience.wiley.com).

ABSTRACT: We present a novel approach to improving organoclay exfoliation in a nonpolar matrix, polyethylene. High-density polyethylene (HDPE) particles were modified by exposure to a reactive gas atmosphere containing F_2 and O_2. This treatment was aimed at increasing the polarity of the polymer with the formation of carboxyl, hydroxy, and ketone functionalities on the particle surface. The surface-treated high-density polyethylene (ST-HDPE) particles were then melt-mixed with an appropriate organoclay to form nanocomposites. Transmission electron microscopy (TEM), wide-angle X-ray scattering, stress–strain analysis, and Izod impact measurements were used to evaluate the nanocomposite morphology and physical properties. These data were compared to those of equivalent nanocomposites prepared from unmodified HDPE and high-density polyethylene grafted with maleic anhydride (HDPE-*g*-MA). The nanocomposites prepared from the ST-HDPE particles exhibited much better properties and organoclay dispersion than those prepared from unmodified HDPE. The level of reinforcement observed in ST-HDPE-based nanocomposites was comparable to, if not better than, that seen in HDPE-*g*-MA-based nanocomposites. However, a comparison of the TEM micrographs suggested better organoclay exfoliation in HDPE-*g*-MA than the current version of ST-HDPE. © 2006 Wiley Periodicals, Inc. J Appl Polym Sci 102: 2980–2989, 2006

Key words: nanocomposites; organoclay; polyethylene (PE)

INTRODUCTION

Polymer-layered silicate nanocomposites formed from the organically modified clay mineral montmorillonite (MMT) and related materials have attracted a great deal of technological and scientific interest in the past decade. These composites offer the promise of greatly improved mechanical,[1–4] thermal,[5,6] and barrier[7,8] properties over those of the matrix polymer because of the nanoscale reinforcement and constraints of the polymer caused by the dispersion of the 1-nm-thick, high-aspect-ratio clay layers. The central scientific issue is how to achieve a high level of dispersion and ultimately full exfoliation of the clay platelets within the polymer matrix because this is necessary to realize large filler aspect ratios. Although several factors play a role in organoclay exfoliation, it seems to be largely dependent on a complex array of interactions between the polymer matrix and the organoclay. Recently, there has been a strong commercial drive for producing such nanocomposites from low-cost polymers such as polyolefins. Unfortunately, polyolefins are highly inefficient at exfoliating organoclays by themselves because there is no favorable interaction with the polar aluminosilicate surface of the clay. Hence, the use of an appropriate compatibilizer or chemical modification of the polymer matrix is required to attain acceptable levels of organoclay exfoliation. The grafting of maleic anhydride to the polyolefin backbone for use as the matrix polymer or as a compatibilizer significantly increases the polarity and thus improves exfoliation in polypropylene (PP)[9,10] and polyethylene (PE).[11–13] Another approach is to copolymerize the olefin monomer with polar monomers such as methacrylic acid[14] or acrylic acid. Ionomers, in which some of the acid groups of such acid copolymers are neutralized to form sodium, zinc, or magnesium salts, offer an extension of this option. The use of ionomers of PE,[15] PP,[16] and a variety of thermoplastics[17–19] as matrices or compatibilizers to prepare nanocomposites with high levels of organoclay dispersion has been reported in the literature.

In this article, we present a novel method for improving organoclay exfoliation in PE. The polarity of high-density polyethylene (HDPE) was increased by the subjection of HDPE particles to a fluoro-oxidation process, which is alternatively known as a reactive-gas surface treatment. These surface-treated high-density polyethylene (ST-HDPE) particles were then melt-mixed with an appropriate organoclay to form nanocomposites with improved levels of exfoliation.

Correspondence to: R. K. Shah (rhutesh@che.utexas.edu) or D. R. Paul (drp@che.utexas.edu).

TABLE I
Materials

Material	Supplier designation	Specifications	Supplier
Unmodified HDPE	HiD 9055	Density = 0.95, melt flow index = 55	Chevron Phillips Chemical Co. (Bartlesville, OK)
HDPE-*g*-MA	Fusabond E MB265D	Density = 0.95, melt flow index = 12.3	DuPont (Wilmington, DE)
ST-HDPE	Inhance HD-1800	Density = 0.95, melt flow index = 50	Inhance Fluoro-Seal (Houston, TX)
$M_2(HT)_2$[a]	Cloisite 20A	Organic loading = 95 mequiv/100 g of clay, organic concentration = 39.6%	Southern Clay Products (Gonzales, TX)

[a] The substituents on the quaternary ammonium compound used to form the organoclay are identified with this shorthand notation: M is methyl, and HT is hydrogenated tallow. Tallow is a natural product composed predominantly (63%) of saturated and unsaturated C_{18} chains. HT is the saturated form yet still contains a small fraction of double bonds.

Transmission electron microscopy (TEM), wide-angle X-ray scattering (WAXS), stress–strain analysis, and Izod impact measurements were used to evaluate the nanocomposite morphology and physical properties. In addition, these data were compared with those of equivalent nanocomposites prepared from unmodified HDPE and high-density polyethylene grafted with maleic anhydride (HDPE-*g*-MA).

EXPERIMENTAL

Materials

A brief description of the materials used in this study is given in Table I. ST-HDPE was prepared by the subjection of 18-μ HDPE particles to a reactive gas atmosphere containing F_2 and O_2, a process sometimes termed fluoro-oxidation. This treatment functionalizes the surface so that it has a composition of 10–15 atom % fluorine and 10–15 atom % oxygen. The surface modification was characterized with Fourier transform infrared (FTIR) spectroscopy. Figure 1(a) compares the FTIR spectra of ST-HDPE and unmodified HDPE (before the surface treatment). The two spectra look similar, except in the carbonyl region (1600–1800 cm^{-1}). For clarity, this part of the spectra is expanded in Figure 1(b). It appears that the fluoro-oxidation process results in the formation of carboxyl, aldehyde, and ketone functionalities on the particle surface. These polar groups create a very high surface energy on the particles that is in excess of 60 dyn/cm and enables the particles to be wet by and completely dispersed in water. The treatment essentially follows a free-radical mechanism. Crosslinking of the surface molecules on the particles occurs in concert with the treatment. Differential scanning calorimetry analysis of the samples suggests that the crystallinity of HDPE is not affected by the surface treatment. Besides ST-HDPE, commercially available HDPE (without any modifications) and HDPE-*g*-MA with similar specifications were also used as matrices in this study for comparison.

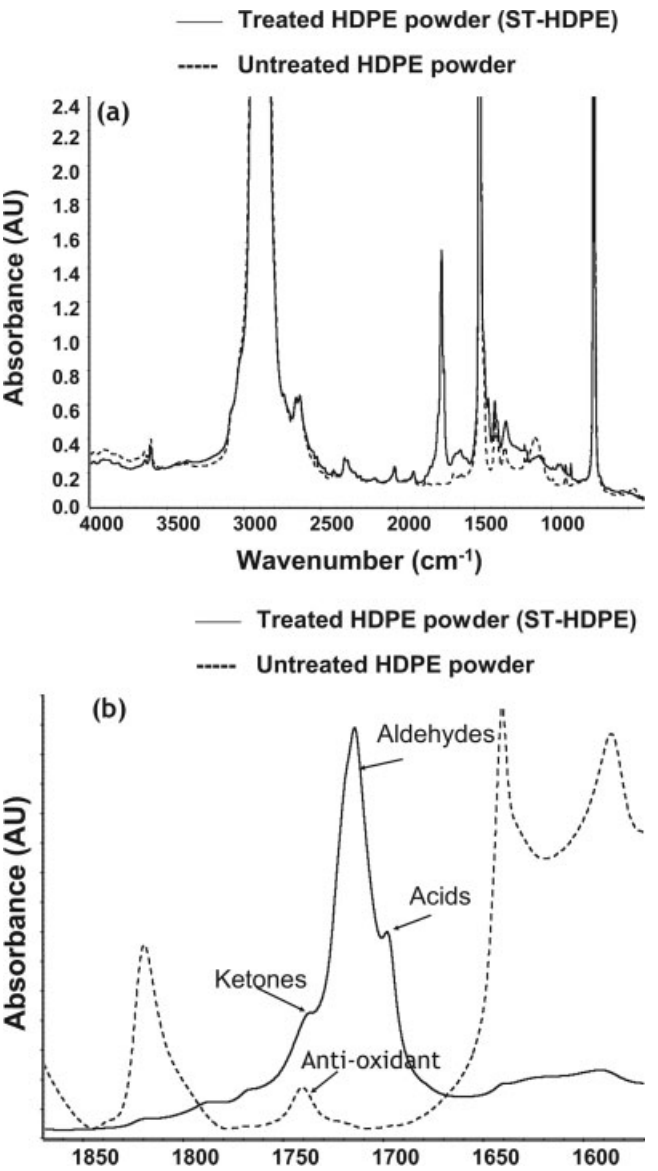

Figure 1 (a) FTIR spectra of ST-HDPE and parent HDPE (unmodified) and (b) the same spectra plotted with an expanded wave-number scale to highlight the carbonyl region of the spectra. The absorbance scale of the spectrum for unmodified HDPE is also expanded for clarity.

The organically modified clay, designated here as $M_2(HT)_2$, was generously donated by Southern Clay Products (Gonzalez, TX) and was used as received. It was prepared by a cation-exchange reaction between sodium montmorillonite and the surfactant dimethyl bis(hydrogenated tallow) ammonium chloride (Arquad 2HT-75). The choice of the organoclay was based on a recent study exploring the effect of the surfactant structure on organoclay exfoliation in PE-type matrices,[14,15] which revealed that greater exfoliation could be achieved with surfactants with multiple alkyl tails on the ammonium ion rather than one tail.

Melt processing

Nanocomposites were prepared by the melt mixing of the polymers with organoclay powder in a Haake corotating, intermeshing, twin-screw extruder (diameter = 30 mm, length/diameter = 10) with a barrel temperature of 160°C, a screw speed of 280 rpm, and a feed rate of 1200 g/h (Thermo-electron corporation, Waltham, MA). The selection of the extrusion temperature was based on a prior study that revealed that in PE–organoclay nanocomposites surfactant degradation increases when melt processing is performed at temperatures higher than 175°C.[20] Also, the low extrusion temperature helped to increase the melt viscosity of these low-molecular-weight, injection-molding-grade polymers. The higher melt viscosity also imparted sufficient melt strength to the extrudate strand for continuous pelletization. After extrusion, the amount of MMT in each nanocomposite was determined by the placement of predried nanocomposite pellets in a furnace at 900°C for 45 min and the weighing of the remaining MMT ash.

Tensile specimens (ASTM D 638) and Izod specimens (ASTM D 256) were prepared via injection molding with an Arburg Allrounder 305-210-700 injection-molding machine with a barrel temperature of 160°C, a mold temperature of 45°C, an injection pressure of 40 bar, and a holding pressure of 40 bar (Lossburg, Germany). After the molding, the samples were immediately sealed in a PE bag and placed in a vacuum desiccator for a minimum of 24 h before testing.

Testing and characterization

Tensile tests were conducted at room temperature according to ASTM D 696 with an Instron model 1137 machine equipped with digital-data-acquisition capability (Norwood, MA). The modulus was measured with an extensiometer at a crosshead speed of 0.51 cm/min, whereas the elongation at break was measured at crosshead speeds of 0.51 and 5.1 cm/min. It was not possible to measure elongations greater than 400% because of equipment limitations. Typically, data from six specimens were averaged to determine the tensile properties with standard deviations on the order of 1–5% for the modulus, 0–2% for the tensile strength, and 0–21% for the elongation at break. Notched Izod impact tests were performed at room temperature with a TMI Izod tester (6.8-J hammer and 3.5 m/s impact velocity) according to ASTM D 256. It is a common practice to cut Izod bars in half (to generate more samples) and average the impact strength data from the gate end (the end at which the molten polymer enters the mold during injection molding) and the far end. However, in multicomponent systems, morphological differences can lead to significant differences between the impact strength measured at the gate end and far end of a sample. Hence, in this study, the impact strength data from four samples each from the gate end and from the far end of the bar were averaged separately; the standard deviation of these values was in the range of 0–20%.

WAXS was conducted with a Sintag XDS 2000 diffractometer in the reflection mode with an incident X-ray wavelength of 1.542 Å at a scanning rate of 1.0°/min (Scintag, Inc., Cupertino, CA). X-ray analyses were performed at room temperature on injection-molded Izod bars. The specimens were oriented so that the incident beam reflected off the major face.

Samples for TEM analysis were taken from the core portion of an Izod bar parallel to the flow direction but perpendicularly to the major face. Ultrathin sections approximately 50 nm thick were cut with a diamond knife at a temperature of −60°C with an RMC PowerTome XL microtome (Boeckeler Instruments Inc., Tucson, AZ). Sections were collected on 300-mesh grids and subsequently dried with filter paper. These were then examined with a JEOL 2010F TEM instrument equipped with a field emission gun at an accelerating voltage of 120 kV. The negative films containing the electron micrographs were electronically scanned and converted into gray-scale tagged-image file format (TIFF) image files. To conduct a quantitative analysis on these images, the TIFF files were opened in Adobe Photoshop, with which the dimensions of the dispersed platelets and agglomerates were traced over into an overlapped blank layer. Two separate tracings were performed for each TEM picture: one contained the lengths of the particles, and the other one contained their thicknesses. The resulting black and white layer files were then imported into image analysis software (SigmaScan Pro), which analyzed the traced particles, assigned a numerical label to each of them, and exported their characteristic dimensions to a different file. Because two different tracings were used for measuring the lengths and thicknesses of the particles, each particle was assigned two different numerical labels. This made it extremely

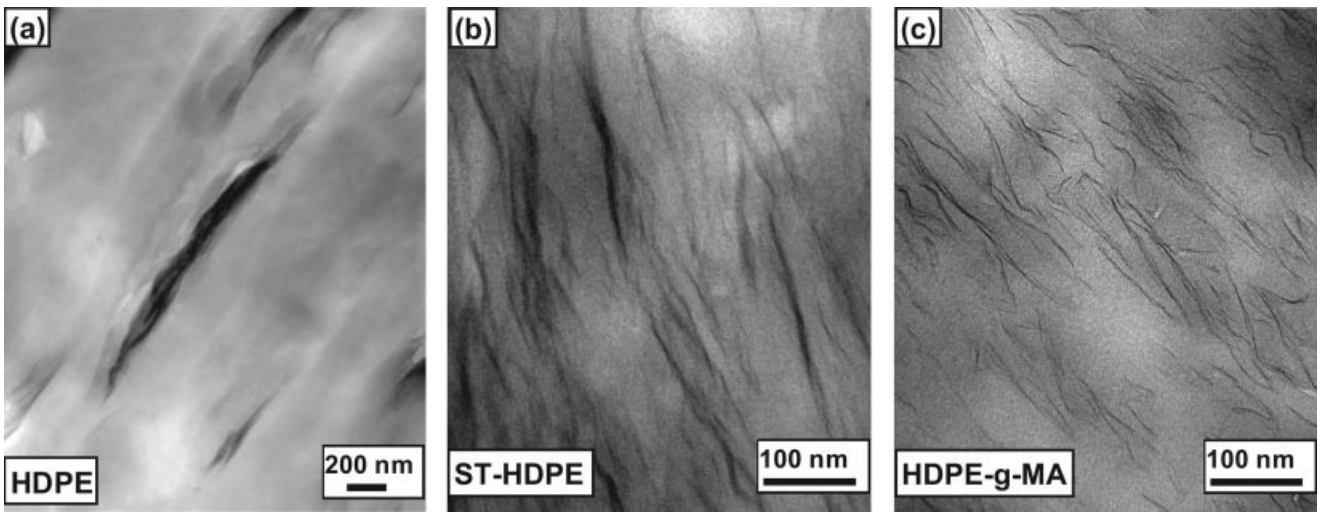

Figure 2 TEM micrographs of nanocomposites prepared from $M_2(HT)_2$ organoclay and (a) unmodified HDPE, (b) ST-HDPE, and (c) HDPE-*g*-MA. The concentration of MMT in all three cases was ~ 5 wt %. The samples were taken from the core portion of an Izod bar and viewed parallel to the flow direction but perpendicularly to the major face.

difficult to match the length of a given particle with its thickness, and thus calculate its aspect ratio. Hence, in this study, the aspect ratio of the particles for any given nanocomposite was determined by the division of its average particle length by its average particle thickness.

RESULTS AND DISCUSSION

Morphological characterization with TEM and particle analysis

Figure 2 shows TEM micrographs comparing the morphologies of nanocomposites formed from the $M_2(HT)_2$ organoclay and HDPE, ST-HDPE, and HDPE-*g*-MA matrices. Nanocomposites from ST-HDPE [Fig. 2(b)] and HDPE-*g*-MA [Fig. 2(c)] exhibited a much higher level of clay exfoliation and distribution than those made from unmodified HDPE [Fig. 2(a)]. Of the two modifications of the HDPE matrix, HDPE-*g*-MA seemed to exfoliate the organoclays better than ST-HDPE. The micrographs of nanocomposites prepared from the former reveal a pattern of uniformly dispersed single platelets along with a few, thin bundles comprising two to three platelets. On the other hand, the morphology of ST-HDPE/$M_2(HT)_2$ nanocomposites, though much more exfoliated than HDPE/$M_2(HT)_2$ nanocomposites, revealed thicker bundles comprising five to eight platelets.

To provide a quantitative comparison of the level of organoclay exfoliation in the three matrices, particle analysis was conducted on TEM micrographs of the nanocomposites. For best statistical validity, a substantial number of particles (>300) should be analyzed for a given nanocomposite. This was not possible for the poorly exfoliated HDPE/$M_2(HT)_2$ nanocomposites as each of their TEM micrographs barely contained five to six large agglomerates. Hence, for this study, the length and thickness of 28 particles were determined for HDPE/$M_2(HT)_2$ nanocomposites, whereas 348 and 421 particles for ST-HDPE/$M_2(HT)_2$ and HDPE-*g*-MA/$M_2(HT)_2$ nanocomposites, respectively, were analyzed with particle analysis software (see Table II).

Figure 3 shows a series of histograms of MMT particle lengths and pertinent statistical data obtained on nanocomposites containing ~ 5 wt % MMT prepared from $M_2(HT)_2$ organoclay and the three HDPE-based matrices. The sections were taken parallel to the flow

TABLE II
Particle Analysis Results

Organoclay nanocomposite	Number of particles analyzed	Number-average particle length (nm)	Weight-average particle length (nm)	Number-average particle thickness (nm)	Weight-average particle thickness (nm)	Aspect ratio[a]	Aspect ratio[b]
HDPE/5.2 wt % MMT	28	548.0	806.8	73.1	130.1	7.5	6.2
ST-HDPE/5.55 wt % MMT	348	114.5	149.0	6.5	8.8	17.5	17.0
HDPE-*g*-MA/4.97 wt % MMT	421	53.0	68.0	1.9	2.7	28.4	25.5

[a] Computed from the number-average platelet lengths ($\bar{l}_n$) and thicknesses ($\bar{t}_n$).
[b] Computed from the weight-average platelet lengths ($\bar{l}_w$) and thicknesses ($\bar{t}_w$).

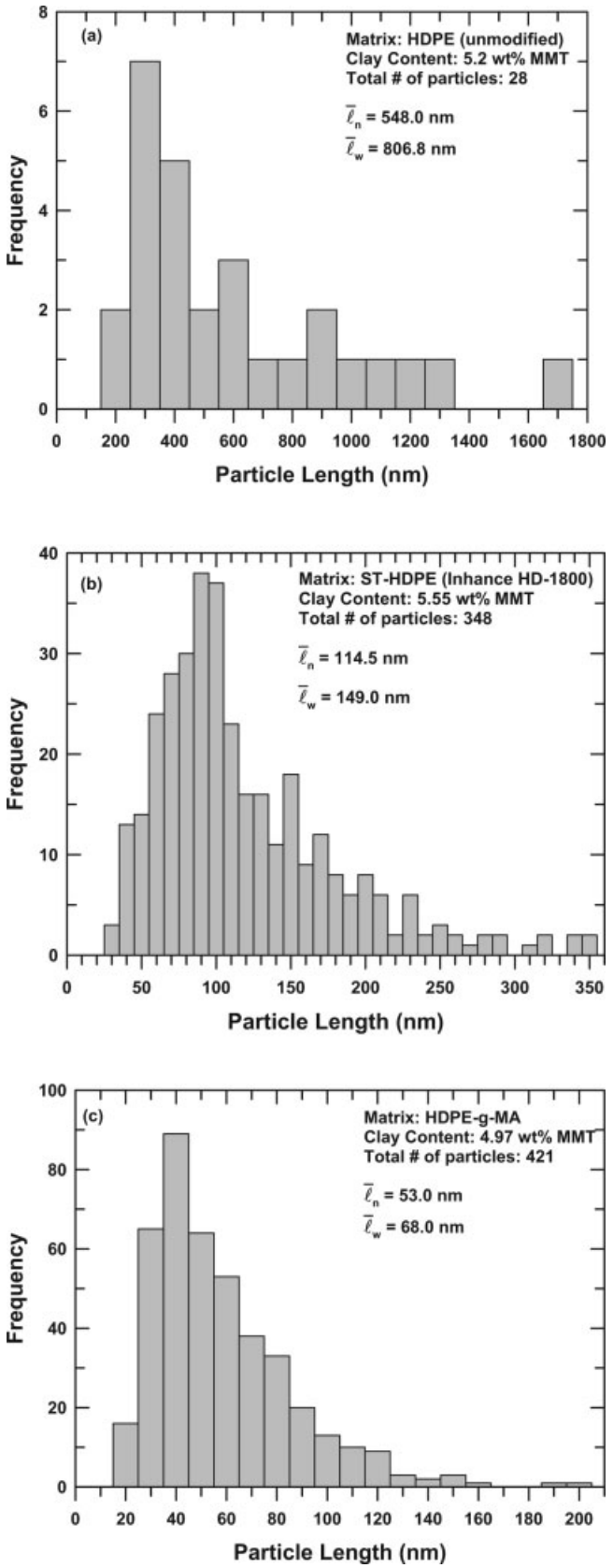

Figure 3 Histograms of the MMT particle length obtained by an analysis of TEM micrographs of nanocomposites containing ~ 5 wt % MMT prepared from (a) unmodified HDPE, (b) ST-HDPE, and (c) HDPE-*g*-MA.

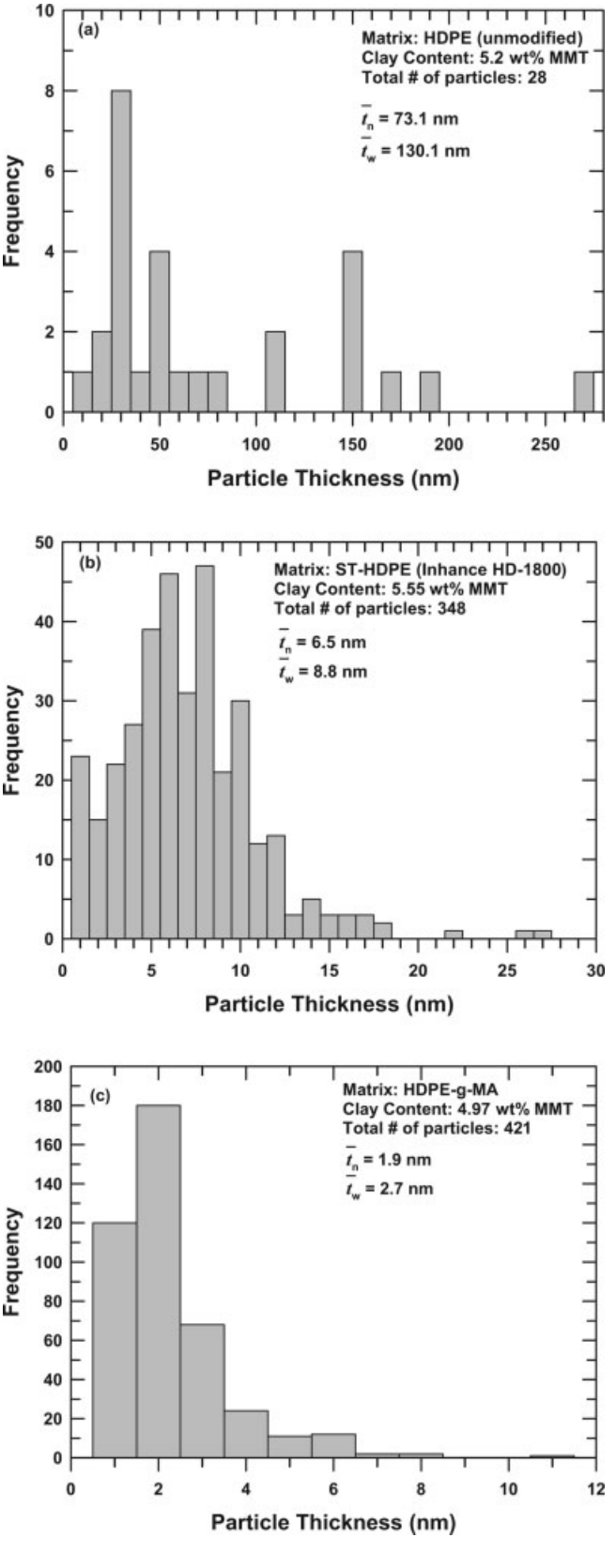

Figure 4 Histograms of the MMT particle thickness obtained by an analysis of TEM micrographs of nanocomposites containing ~ 5 wt % MMT prepared from (a) unmodified HDPE, (b) ST-HDPE, and (c) HDPE-*g*-MA.

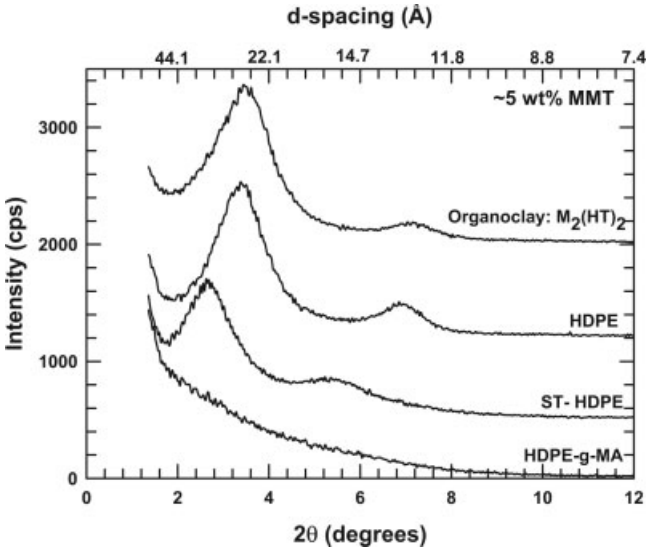

Figure 5 WAXS patterns of nanocomposites prepared from $M_2(HT)_2$ organoclay and the three HDPE-based matrices. The concentration of MMT in all cases was ~ 5 wt %. The X-ray pattern of the $M_2(HT)_2$ organoclay has been plotted for comparison. The curves have been shifted vertically for clarity.

direction but perpendicularly to the major face. Similar measurements were conducted for the thickness of the clay particles, and the results are plotted in Figure 4. As expected, the filler particle size in HDPE-*g*-MA- and ST-HDPE-based nanocomposites was much smaller than that in HDPE-based nanocomposites. The average particle length of 53 nm calculated for the HDPE-*g*-MA nanocomposites agreed well with the average particle length in well-exfoliated nylon 6 nanocomposites determined with a similar technique.[21] The average particle thickness of 1.9 nm for HDPE-*g*-MA nanocomposites roughly corresponded to the thickness of two MMT platelets and was slightly higher than the 1.5 nm thickness reported for nylon 6 nanocomposites.[21] This suggests that although the HDPE-*g*-MA-based nanocomposites revealed a fairly exfoliated morphology, the level of exfoliation was not as high as that seen in nanocomposites prepared from high-molecular-weight nylon 6. The average thickness of the filler particles in the ST-HDPE nanocomposites was calculated to be 6.5 nm, which was a little higher than that of HDPE-*g*-MA nanocomposite particles but significantly lower than that of the 73-nm-thick particles observed in HDPE-based nanocomposites. The average particle length in ST-HDPE nanocomposites was greater than that in HDPE-*g*-MA (114 vs 53 nm). This could be the result of partially sheared clay agglomerates and/or skewing of thicker clay bundles, as described by Chavarria and Paul.[21] The aspect ratio of the particles in each nanocomposite was calculated by the division of the average particle length by the av-

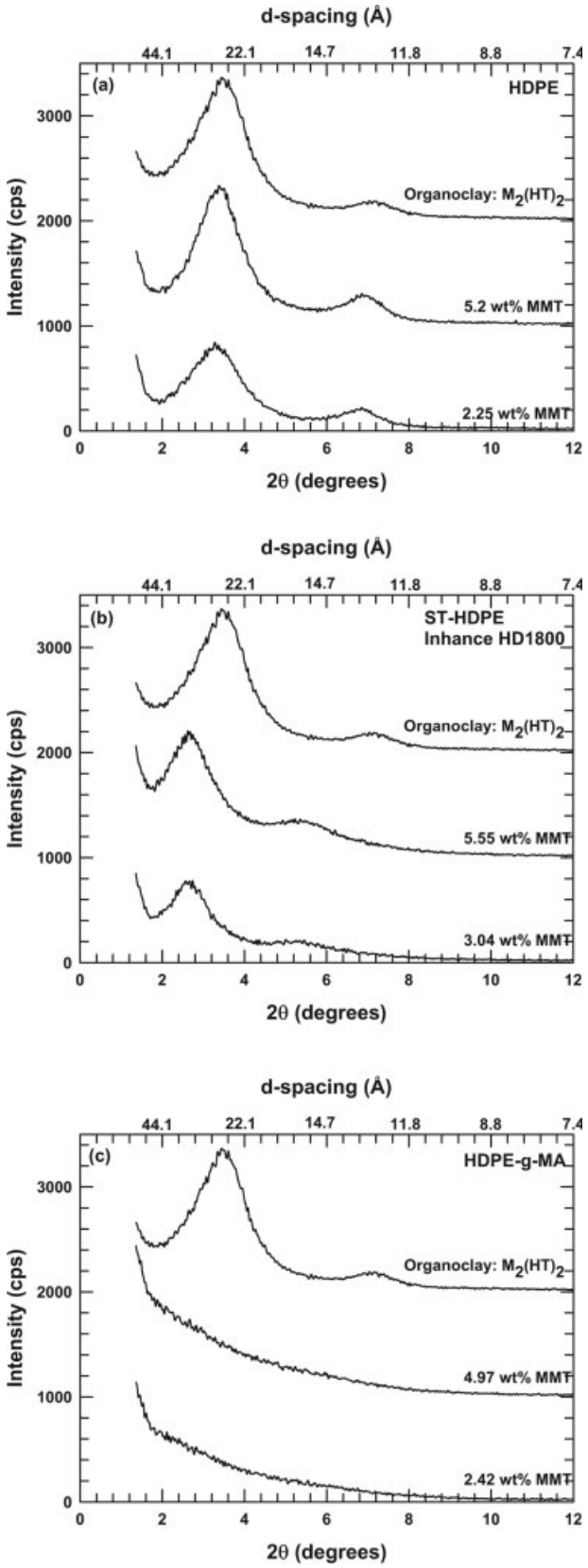

Figure 6 WAXS patterns of nanocomposites prepared from $M_2(HT)_2$ organoclay and (a) unmodified HDPE, (b) ST-HDPE, and (c) HDPE-*g*-MA. The X-ray pattern of the $M_2(HT)_2$ organoclay has been plotted for comparison. The curves have been shifted vertically for clarity.

erage particle thickness of the nanocomposite (see Table II). Of the three matrices, HDPE-*g*-MA nanocomposite particles had the highest aspect ratio, followed by ST-HDPE, whereas the HDPE composite particles had the lowest aspect ratio. On the basis of the TEM evaluation and particle analysis, we safely concluded that the two matrix modification methods employed in this study significantly improved the organoclay dispersion in comparison with a virgin PE matrix. However, HDPE-*g*-MA apparently exfoliated the organoclays better than the current version of ST-HDPE.

WAXS analysis of the nanocomposites

Figure 5 compares the WAXS scans of the $M_2(HT)_2$ organoclay and its nanocomposites prepared through melt mixing with three HDPE-based matrices. The organoclay pattern reveals an intense peak around $2\theta = 3.46^\circ$ corresponding to a basal spacing of 25.5 Å. The X-ray pattern for the HDPE-*g*-MA-based nanocomposites does not show a characteristic basal reflection, and this is often interpreted as a sign of complete exfoliation. However, we believe that this lack of an X-ray peak is the result of a combination of high levels of dispersion and a more random orientation of clay particles rather than an indication of a completely exfoliated morphology. The TEM analyses support this hypothesis. The X-ray scan for HDPE-based nanocomposites reveals a distinct peak indicative of the presence of unexfoliated clay tactoids. The peak position is the same as that of the pristine organoclay, and this suggests that the organoclay interplatelet distances were unaltered during the formation of these composites. On the other hand, the WAXS peak of the ST-HDPE nanocomposite shifted to a higher *d*-spacing than the organoclay; according to prevalent interpretations in the literature suggests the intercalation of the polymer within the clay galleries.

The position of the peak (or the lack of it) does not change along with the organoclay content of the nanocomposites, as shown in Figure 6. Nanocomposites made from low-density polyethylene[20] and poly (ethylene-*co*-methacrylic acid) ionomers[15] exhibit similar trends.

Mechanical properties

Selected mechanical properties of nanocomposites prepared from $M_2(HT)_2$ organoclay and the three HDPE-based matrices are listed in Table III. Figure 7(a) compares the tensile modulus of the different nanocomposites as a function of their MMT content. To account for the differences between the moduli of the three matrices, the relative improvement in the stiffness achieved by the melt mixing of these polymers with the $M_2(HT)_2$ organoclay is presented in Figure 7(b). The increase in the modulus observed in the nanocomposites prepared from ST-HDPE and HDPE-*g*-MA matrices is much stronger than that observed in the nanocomposites prepared from unmodified HDPE. However, the level of reinforcement observed in ST-HDPE-based nanocomposites is comparable to, if not better than, that seen in HDPE-*g*-MA-based nanocomposites. Thus, it seems that the modulus data are not in complete agreement with the nanocomposite morphology, as revealed by TEM and WAXD analysis. This could be a result of possible differences between the filler orientation in ST-HDPE- and HDPE-*g*-MA-based nanocomposites. The tensile modulus of a nanocomposite sample is a function of the level of organoclay exfoliation and the orientation of the aluminosilicate platelets in the direction of the axial force. If the platelet orientation in HDPE-*g*-MA-based nanocomposites is more random than in ST-HDPE-based nanocomposites, their tensile moduli would not be as high as what one might expect from their filler aspect ratio. This could also explain why the WAXD patterns of HDPE-*g*-MA-based nanocomposites are devoid of any peaks despite the presence of a few doublets and triplets, as revealed by their

TABLE III
Selected Mechanical Properties of Nanocomposites Prepared by Melt Processing

Polymer	Clay loading (wt % MMT)	Modulus (GPa)	Relative modulus	Tensile strength at 0.51 cm/min (MPa)	Elongation at break (%)		Izod impact strength (J/m)	
					0.51 cm/min	5.1 cm/min	Gate end	Far end
HDPE	0.00	0.595	1.000	15.6	333.7	88.8	29.4	28.8
HDPE	2.25	0.678	1.139	16.3	15.7	12.1	20.6	20.6
HDPE	5.20	0.768	1.291	16.3	12.5	8.9	19.6	19.1
ST-HDPE	0.00	0.958	1.000	20.3	12.4	8.9	22.5	21.5
ST-HDPE	3.04	1.466	1.530	21.1	4.0	3.6	12.2	9.8
ST-HDPE	5.55	1.942	2.027	21.1	2.8	2.5	13.7	9.8
HDPE-*g*-MA	0.00	0.803	1.000	18.3	>400	>400	71.2[a]	51.7[a]
HDPE-*g*-MA	2.25	1.141	1.421	21.8	>400	328.7	39.8	33.4
HDPE-*g*-MA	4.97	1.399	1.742	23.6	40.9	7.1	46.3	28.4

[a] Ductile failure. All other samples had brittle failure.

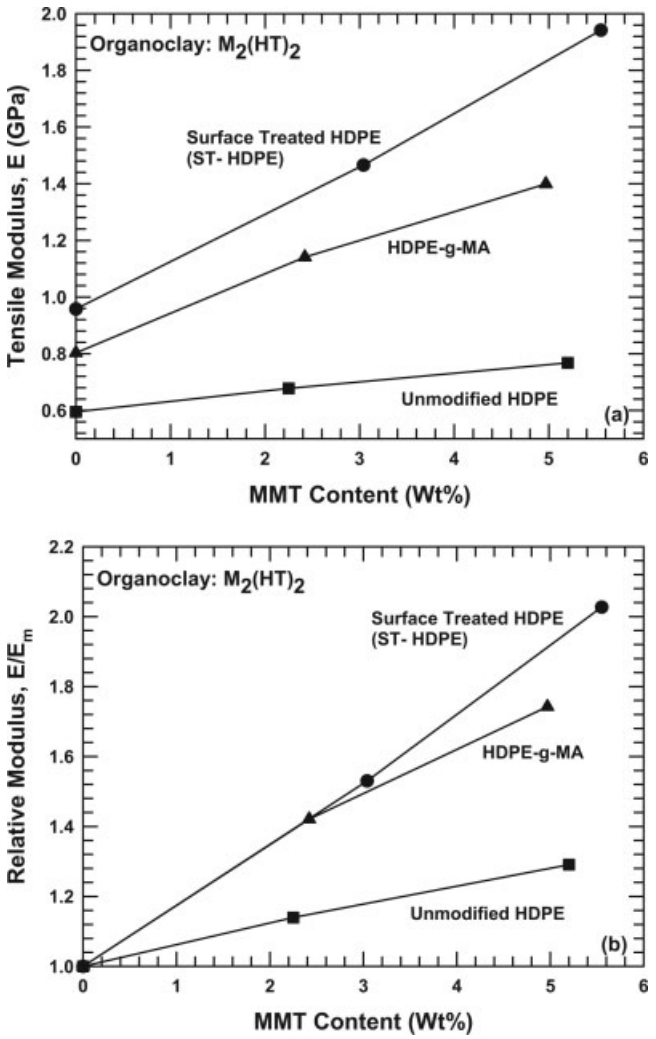

Figure 7 (a) Tensile modulus and (b) relative modulus of nanocomposites prepared from unmodified HDPE, ST-HDPE, and HDPE-*g*-MA.

TEM micrographs. Then again, we are not quite sure what could possibly lead to such differences between the filler orientation in the two composite systems. Hotta and Paul[11] reported a similar discrepancy between the tensile properties and TEM morphology of nanocomposites prepared from linear low-density polyethylene (LLDPE) and maleic anhydride grafted linear low-density polyethylene (LLDPE-*g*-MA). In their study, nanocomposites prepared from LLDPE-*g*-MA revealed a very well exfoliated morphology in comparison with those prepared from LLDPE. However, the mechanical properties of the two nanocomposite systems did not reflect this large difference in the morphology to the extent expected.

The relationship between the MMT content of the nanocomposites and the elongation at break is shown in Figure 8 for two rates of extension. It is interesting to note the differences in the elongation at break for the three unfilled polymers. The samples prepared from ST-HDPE exhibited much lower ductility than those prepared from unmodified HDPE with similar specifications. As expected, the ductility of all polymers decreased along with an increase in the MMT content.

The effects of the clay content on the room-temperature Izod impact behavior of nanocomposites prepared from HDPE, ST-HDPE, and HDPE-*g*-MA matrices are presented in Figure 9. For all the nanocomposites, toughness as judged by Izod deteriorated gradually with increasing clay concentration. There was not much difference between the trends observed in the gate- and far-end samples. However, the gate-end samples did appear to be a little tougher than the far-end samples (for both the neat polymer and nanocomposites). Although ST-HDPE and its nanocomposites were significantly less ductile than HDPE and composites made from it, there was not much differ-

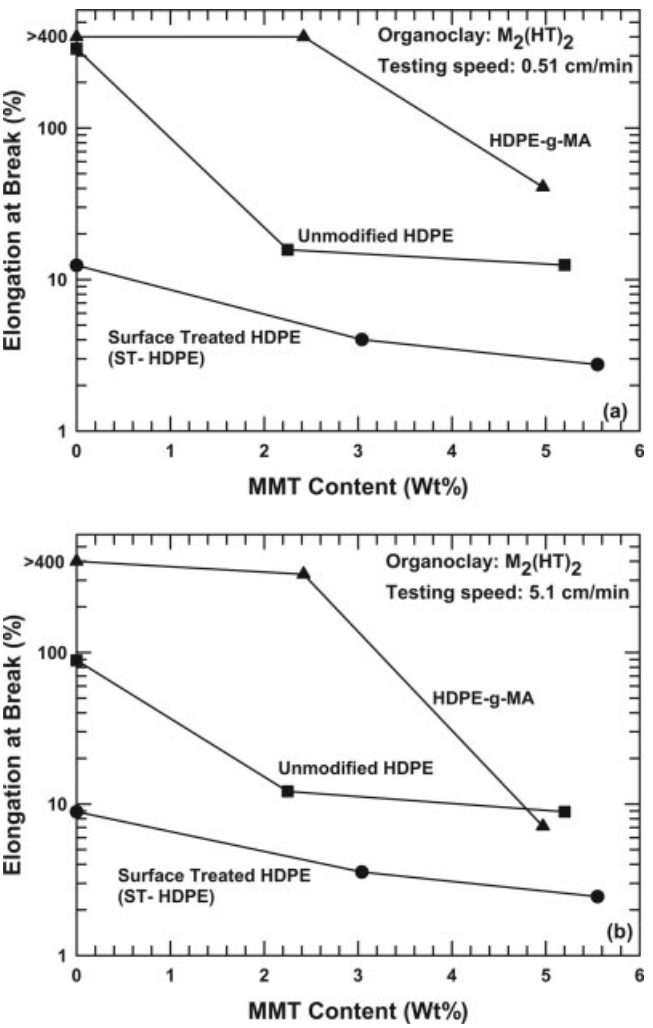

Figure 8 Elongation at break measured at crosshead speeds of (a) 0.51 and (b) 5.1 cm/min for nanocomposites prepared from unmodified HDPE, ST-HDPE, and HDPE-*g*-MA.

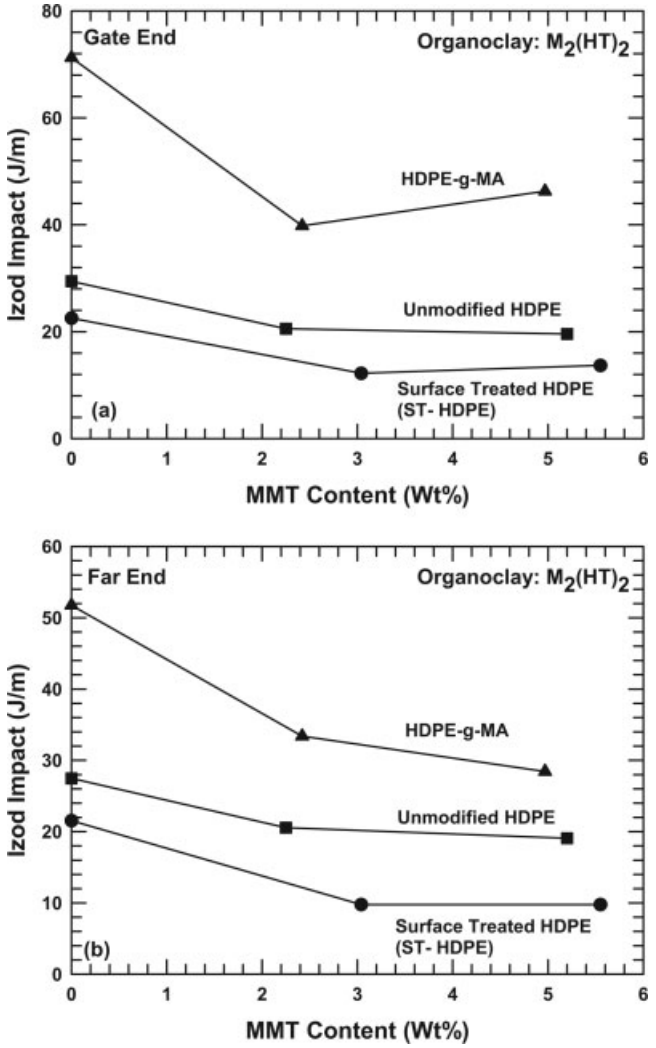

Figure 9 Izod impact strength of (a) gate-end and (b) far-end samples of nanocomposites prepared from unmodified HDPE, ST-HDPE, and HDPE-*g*-MA.

ence between their Izod impact values. This could be attributed to the differences in the moduli of the two sets of materials. Because the Izod measures the energy absorbed during impact, that is, the area under the curve of the resisting force versus the displacement during the test, the values obtained reflect a net result of opposing effects brought by higher stiffness and lower ductility. In our case, the higher modulus of ST-HDPE and its nanocomposites somewhat compensated for the lowering effects (in terms of the Izod impact strength) caused by their poor ductility (compared with unmodified HDPE).

CONCLUSIONS

A novel method for improving organoclay exfoliation in PE has been presented here. The polarity of the HDPE matrix was increased by the subjection of the PE particles to a controlled fluoro-oxidation process; this formed hydroxyl, carboxyl, and ketone functionalities on the surface of the polymer particles. These ST-HDPE particles were then melt-mixed with an appropriate organoclay to form nanocomposites, whose morphology and properties were compared to those of nanocomposites prepared from unmodified HDPE and HDPE-*g*-MA. The level of reinforcement observed in ST-HDPE-based nanocomposites was comparable to, if not better than, that seen in HDPE-*g*-MA-based nanocomposites. TEM micrographs of HDPE-*g*-MA- and ST-HDPE-based nanocomposites revealed a much more exfoliated morphology than that of nanocomposites prepared from unmodified HDPE. However, the level of exfoliation observed in HDPE-*g*-MA by TEM was better than that observed in the current version of ST-HDPE.

This was our first effort at using a surface treatment as a means of improving organoclay dispersion in PE. It would be interesting to raise the polarity of the particles even further by an increase in the intensity of the oxidative treatment, that is, an increase in the thickness of the surface-treatment layer of the PE particle. We expect this to further elevate the level of organoclay exfoliation in ST-HDPE. The effect of the molecular weight of ST-HDPE particles on the level of organoclay exfoliation should also be examined with a low-melt-index (higher molecular weight) ST-HDPE sample. The eventual goal is to use such surface-treated particles as compatibilizers (e.g., PE-*g*-MA) to prepare PE nanocomposites on a commercial scale. From a technical standpoint, this requires the miscibility of the surface-treated PE in unmodified PE. If this miscibility could be achieved, then highly concentrated organoclay/HDPE master batches, with high levels of exfoliation, could be prepared and subsequently diluted with unmodified PE (while preserving exfoliation).

The authors sincerely thank Chevron Phillips Chemical Co. and DuPont for donating samples of high-density polyethylene and high-density polyethylene grafted with maleic anhydride, respectively. They are also thankful to Southern Clay Products, Inc., for providing organoclay materials and wide-angle X-ray diffraction analyses. The authors acknowledge Shane Burgan for his help during melt processing and J. P. Zhou for his help with transmission electron microscopy.

References

1. Wang, Z.; Pinnavaia, T. J. Chem Mater 1998, 10, 3769.
2. Lan, T.; Pinnavaia, T. J. Chem Mater 1994, 6, 2216.
3. Liu, L.; Qi, Z.; Zhu, X. J Appl Polym Sci 1999, 71, 1133.
4. Usuki, A.; Koiwai, A.; Kojima, Y.; Kawasumi, M.; Okada, A.; Kurauchi, T.; Kamigaito, O. J Appl Polym Sci 1995, 55, 119.

5. Vaia, R. A.; Price, G.; Ruth, P. N.; Nguyen, H. T.; Lichtenhan, J. J. Appl Clay Sci 1999, 15, 67.
6. Gilman, J. W. Appl Clay Sci 1999, 15, 31.
7. Messersmith, P. B.; Giannelis, E. P. J Polym Sci Part A: Polym Chem 1995, 33, 1047.
8. Yano, K.; Usuki, A.; Okada, A.; Kurauchi, T.; Kamigaito, O. J Polym Sci Part A: Polym Chem 1993, 31, 2493.
9. Hasegawa, N.; Kawasumi, M.; Kato, M.; Usuki, A.; Okada, A. J Appl Polym Sci 1998, 67, 87.
10. Lee, H.-S; Fasulo, P. D.; Rodgers, W. R.; Paul, D. R. Polymer 2005, 46, 11673.
11. Hotta, S.; Paul, D. R. Polymer 2004, 45, 7639.
12. Hasegawa, N.; Okamoto, H.; Kawasumi, M.; Kato, M.; Tsukigase, A.; Usuki, A. Macromol Mater Eng 2000, 280, 76.
13. Li, X.; Wang, C.-Y.; Fang, L.; Liu, L.-Z. Harbin Ligong Daxue Xuebao 2003, 8, 90.
14. Shah, R. K., Ph.D. Dissertation, The University of Texas at Austin, 2006.
15. Shah, R. K.; Hunter, D. L.; Paul, D. R. Polymer 2005, 46, 2646.
16. Ding, R.-D.; Newell, C. U.S. Pat. 6,861,481 (2005).
17. Barber, G. D.; Carter, C. M.; Moore, R. B. Annu Tech Conf Soc Plast Eng 2000, 58, 3763.
18. Start, P. R.; Mauritz, K. A. J Polym Sci Part B: Polym Phys 2003, 41, 1563.
19. Kovarova, L.; Kalendova, A.; Malac, J.; Vaculik, J.; Malac, Z.; Simonik, J. Annu Tech Conf Soc Plast Eng 2002, 60, 2291.
20. Shah, R. K.; Paul, D. R. Polymer, submitted.
21. Chavarria, F.; Paul, D. R. Polymer 2004, 45, 8501.